

## Electrochemical Investigation and Voltammetric Determination of Hydrazine Based on Organic Modifier and N-Doped Reduced Graphene Aerogel/ Molybdenum Oxide Nanorods Multilayer Nanocomposite Modified Glassy Carbon Electrode

Mohammad Mazloum-Ardakani\*, Hamed Aarabi-Ardakani, Zahra Alizadeh, Mahnoosh Haghsheenas, Fatemeh Farbod, Sahar Saadat HosseiniKhah, BiBi Fatemeh Mirjalili

Department of Chemistry, Faculty of Science, Yazd University, Yazd, Iran

Received: 16 January 2022

Accepted: 13 February 2022

DOI: 10.30473/ijac.2022.63882.1236

### Abstract

In this research, a novel modified glassy carbon electrode (GCE) was successfully fabricated with a tri-component nanocomposite consisting of 5-(3,4-dihydroxyphenyl)8,8-dimethyl-2-(methyl thio)-7,8,9,10-tetrahydropyrimido [4,5-b]quinolone-4,6(3H,5H)-dione (PQ<sub>23</sub>) and Nitrogen-doped reduced graphene oxide aerogel/molybdenum oxide nanorods (PQ<sub>23</sub>/N-doped-rGO/MoO<sub>2</sub>/GCE) as sensing platform toward hydrazine (HDZ). The nanocomposite is characterized by MAP analysis, X-ray diffraction (XRD) analysis, scanning electron microscopy (SEM), and energy-dispersive X-ray spectroscopy (EDS). Through electrochemical investigations, the electron transfer coefficient between PQ<sub>23</sub> and the N-doped-rGO/MoO<sub>2</sub>/GCE (glassy carbon electrode which was modified with reduce graphene oxide decorated by molybdenum oxide nanorods) and the apparent charge transfer rate constant, ks, and diffusion coefficient (D) were calculated. Electrochemical behavior and electrocatalytic activity of the nanocomposite modified GCE were studied by electrochemical impedance spectroscopy (EIS), cyclic voltammetry (CV), and differential pulse voltammetry (DPV). Under the optimum experimental condition, the designed sensor exhibited high sensitivity and suitable selectivity for hydrazine oxidation, enabling the detection of hydrazine with a linear range of 25.0-1000.0  $\mu$ M and a good detection limit ( $3\sigma$ ) was 4.2  $\mu$ M. The designed electrochemical sensor shows good repeatability, reproducibility, and acceptable stability with an RSD less than 3.2%.

### Keywords

Electrochemical Sensor, Graphene Aerogels, Nitrogen-Doped Aerogels, MoO<sub>2</sub>, Hydrazine.

### 1. INTRODUCTION

Hydrazine and its derivatives are widely applied in the chemical and pharmaceutical industries. They are mainly used as antioxidants, explosives, fuel cells, pesticides, herbicides, dyes and synthesis of insecticides. Despite this advantage, hydrazine is a toxic material. Therefore, an easy and sensitive analytical method for the detection of hydrazine is warranted [1–3]. Some analysis methods such as flow injection [4], atomic absorption spectroscopy [5], ion chromatography [6], spectrophotometry [7], high-performance liquid chromatography [8] and electrochemical sensors [9,10] It has been reported to determine HDZ in various samples. But most of these methods are revoluted, time-consuming, costly, low precision, and relatively low linear range. The electrochemical method is of special importance due to its simplicity, high sensitivity and fast response time [11]. However, the electrochemical oxidation of HDZ is kinetically slow and requires high potential at carbon electrodes. Therefore, various approaches to reduce the potential and increase the oxidation response have been investigated [12,13]. Graphene

(Gr) is a two-dimensional (2D) crystal that is stable in ambient conditions. Among the properties of graphene are mechanical strength, high surface area, thermal conductivity and high elasticity. Graphene oxide (GO) is a main member of the graphene family, which is fabricated by ultrasonic peeling of graphite oxide plates in water. The most remarkable property of GO is that it can be partially reduced to graphene by eliminating oxygenated groups [14,15]. Doping of graphene carbon network with heteroatoms (eg B, N and P) increases the electrical conductivity as well as the hydrophilicity and creates electro-catalytically active sites on the surface. In addition, nitrogen doping can create remarkable properties such as selective sensitivity to electrochemical catalytic activity and adsorbents [16]. Metal nanoparticles have received a large deal of attention due to their outstanding attributes and applications in the fields of catalysis, magnetism, biological activity, and electronics [17]. Molybdenum is available in three oxidation states that can easily participate in redox reactions and also have an interesting metal electrical conductivity [18]. Molybdenum oxide

\*Corresponding Author: mazloum@yazd.ac.ir

has unique properties such as chemical stability, rapid redox process and easy preparation of nanoparticles and also has potential applications in chemical synthesis, fueling, capacitors, lithium-ion batteries, gas sensors and other sensors [19]. Recent articles exhibited that some composites based on rGO such as three-dimensional (3D) porous Gr aerogel and glucose oxidase [20], sulfur-functionalized multiple graphene aerogel and Pd@ gold nanoalloys/nitrogen [21], Nitrogen-doped multiple graphene aerogel/gold nanostar [22], Au@ Ag nanoparticle-decorated 3D-N-doped Gr aerogel [23] and porous polypyrrole@ ZIF-8/Gr aerogels [24] could use as a platform in electrochemistry sensors. These nanocomposites based on GO could act as a useful sensing platform for HDZ oxidation reactions. The nanocomposite create an excellent electrochemical sensing platform for various analytes (eg. glucose, HDZ, dopamine,...) and are awaited to have wide potential applications in biosensors and catalysts. In this work 5-(3,4-dihydroxyphenyl)8,8-dimethyl-2-(methylthio)-7,8,9,10-tetrahydropyrimido[4,5-b]quinolone-4,6(3H,5H)-dione (PQ<sub>23</sub>) was engaged as a proper mediator for the oxidation of HDZ at the electrode surface. The nanocomposite PQ<sub>23</sub>/N-doped-rGO/MoO<sub>2</sub> improved the stability, selectivity and sensitivity of the designed sensing platform. CV and Chronoamperometry (CHA) measurements were performed to detect the electrochemical properties of HDZ and to detect its electrocatalytic impact on its oxidation. Finally, the electrochemical performance of the modified electrode (PQ<sub>23</sub>/N-doped-rGO/MoO<sub>2</sub>/GCE) is studied for the detection of HDZ in real samples.

## 2. EXPERIMENTAL

### 2.1 Chemicals and Devices

3,4-Dihydroxybenzaldehyde, dimedone, potassium permanganate, H<sub>2</sub>SO<sub>4</sub>, H<sub>3</sub>PO<sub>4</sub>, HNO<sub>3</sub>, paraphenylenediamine, ammonium heptamolybdate, ethanol, graphite and hydrazine were bought from Merck (Darmstadt, Germany). Distilled water was applied for the fresh provision of all solutions. Morphologies of the nanocomposite PQ<sub>23</sub>/N-doped-rGO/MoO<sub>2</sub> were characterized using SEM (Hitachi S-4160), XRD (X'PertPro, Panalytical Co., Cu Ka), MAP (MIRA3TESCAN-XMU) and EDS (MIRA3TESCAN-XMU) analysis. Electrochemical investigations were done on potentiostat/galvanostat (RADstat-1A, Iran) made by Kian Shar Danesh with the Ivium software package. All experiments were done by a three-electrode system consisting of Ag/AgCl/KCl and a platinum wire was applied as a reference and counter electrodes, respectively. The GCE (Azar

electrode, 3mm diameter) is used as a working electrode. Also, the pH value adjusts with pH meter device (Metrohm 691 model).

### 2.2 Synthesis of organic modifier (PQ<sub>23</sub>)

For the first step, PQ<sub>23</sub> was prepared according to our previous article [25]. In summary, A mixture of 6-amino-2-thioxo-2,3-dihydropyrimidin-4(1H)-one (1 mmol), dimedone (1 mmol), 3,4-dihydroxybenzaldehyde (1 mmol) and Fe<sub>3</sub>O<sub>4</sub>@nano-cellulose/Sb(V) (0.03 g) was stirred by an electrical mortar-heater at 70 °C. The progress of reaction was monitored TLC (n-Hexan:EtOAc, 8:2). After completion of reaction, 5 ml of ethanol was added to the reaction mixture and the catalyst was separated by an external magnet. By cooling of the mixture, the product was appeared as solid which crystallized from EtOH:H<sub>2</sub>O (1:1).

### 2.3 Synthesis of GO

Graphene oxide (GO) was prepared by the modified hummers technique from graphite powder. For this purpose, 1.5 g of graphite powder and 9 g of KMnO<sub>4</sub> were step by step added to the sulfuric acid / phosphoric acid mixture (volume ratio 9: 1) for 30 minutes. The mixture was placed in a sand bath at 50 °C and stirred at this temperature for 12 h. After the reaction time had elapsed, the sand bath was removed and after reaching room temperature, 200 ml of deionized water ice cubes and 3 ml of 30% hydrogen peroxide were added to the obtained mixture. Then, the resulting mixture was centrifuged and the brown precipitate of graphene oxide was washed several times with deionized water. Finally, the precipitates were washed with 100 ml of HCl (30%) solution and then with 100 ml of ethanol. The producing graphite oxide was dried at 50 °C under a vacuum oven for 12 hours. Then, the resulting powder dispersed in deionized water by ultrasound and graphite oxide is converted to graphene oxide [26].

### 2.4 Synthesis of N-doped reduced graphene oxide aerogel

For this synthesis, 0.5 g of GO was dispersed in 30 ml of deionized water by ultrasound. A solution of 1g of paraphenylenediamine in 15 ml of ethanol was prepared separately. This solution was added dropwise to the graphene oxide mixture. The obtained mixture was placed in a water bath at 80 °C and stirred for 30 minutes. Finally, the solution was placed in a Teflon autoclave and heated in a vacuum oven at 180 °C for 12 h. The product black colored composite was washed with ethanol and distilled water and dried in an oven at 60 °C for 12 h [26].

### 2.5 Synthesis of molybdenum oxide nanorods

Initially, a solution of 0.6 mM of ammonium molybdate salt in a volume of 20 ml in deionized water was prepared. Then, the pH of the solution was transferred to the acidic range using nitric acid and the solution was then transferred to an autoclave. The reaction was performed at 160 °C for 12 h [26].

### 2.6 Preparation of N-doped graphene oxide aerogel/molybdenum oxide nanorods composite

To prepare the composite, the mass ratio (1:1) of N-doped graphene oxide aerogel to molybdenum oxide nanorods was weighed and mixed with water and ethanol solvents in a volume ratio (1:1) and placed in an ultrasonic bath for 1 h. Then, it was centrifuged at 2500 rpm for 10 minutes and the final precipitate was dried at 50 °C for 12 hours.

### 2.7 Fabrication of electrochemical sensor

To design the electrochemical sensor, the surface of the GCE was polished with alumina powder on a special cloth and then cleaned with deionized water. In the next step, to activate the electrode surface, sodium bicarbonate (0.1 M) solution was prepared and CV of bare GCE at a scan rate of 100 mV/s in the range of potential (-1.1-1.6) with 20 cycles was performed.

After activation and drying of the electrode surface, the optimum volume of the nanocomposite (1  $\mu$ L) was deposited on the electrode surface to dry and the optimum volume of the modifier (2  $\mu$ L) was then placed on the electrode surface and allowed to dry at 25 °C. Finally, PQ<sub>23</sub>/N-doped-rGO/MoO<sub>2</sub> /GCE sensor was prepared for research.

## 3. RESULT AND DISCUSSION

### 3.1 Characterization of N-doped reduced graphene oxide aerogel/ molybdenum oxide nanorods

To study the composition and structure of GO and N-doped reduced graphene oxide aerogel was used SEM. Fig. (1a) shows the smooth plates and the overlapping, two-dimensional structure of graphene oxide. Fig. (1b) Shows two-dimensional plates and wrinkled graphene layers. The wrinkling increases the surface area on the electrode because shrinkage prevents the sheets from joining and prevents the formation of a graphite structure. Fig. (1c) shows well the molybdenum oxide nanorods.

Some scanning electron microscopes have an EDS system that is used to determine the percentage and identify elements in the sample. Fig. (1d) shows the EDS spectrum with weight and atomic percentages for the elements carbon, nitrogen, oxygen and molybdenum. EDS pattern also shows prominent signals due to carbon, nitrogen, oxygen

and molybdenum, again affirming the successful integration of MoO<sub>2</sub> with graphene.

Mo spectral lines corresponding to permissible transitions from higher to lower levels confirm the presence of molybdenum in the composition. The spectral lines of N, O, and C confirm the presence of rGO doped with nitrogen in the nanocomposite. Fig. (1e) shows the presence and dispersion of molybdenum oxide nanorods on the graphene oxide plates according to the FESEM image and the presence of nitrogen in the reduced graphene oxide plates is observed.

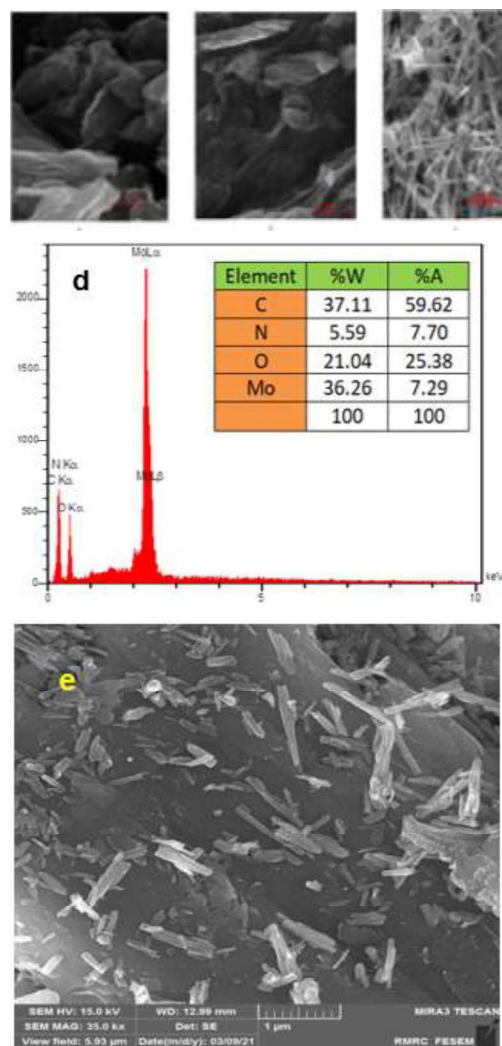


**Fig. 1.** SEM images of a) GO b) N-doped-rGO c) MoO<sub>2</sub> d) EDS Spectrum of N-doped-rGO/MoO<sub>2</sub> e) FESEM of N-doped-rGO/MoO<sub>2</sub>

Fig. (2a) shows a uniform dispersion of molybdenum oxide and nitrogen nanoparticles on the graphene surface according to the MAP image. The XRD spectra of the N-doped reduced graphene aerogel/molybdenum oxide nanorods composite are shown in Fig. (2b). The obtained

diffraction pattern is consistent with the reported references of the MoO<sub>2</sub> composition [26]. The background is seen in Fig. (2b) is due to the amorphous carbon present in the sample.

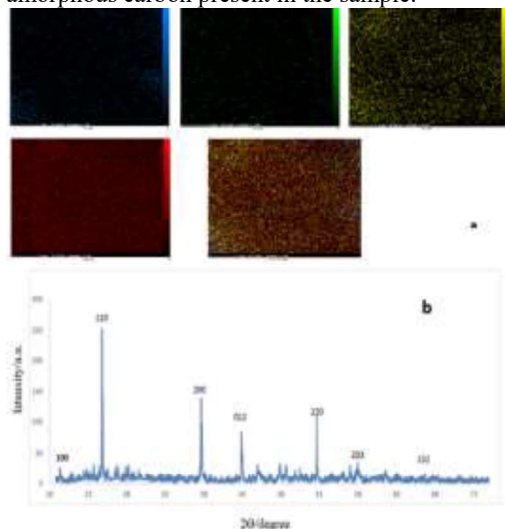


**Fig. 2.** a) MAP of N-doped-rGO/MoO<sub>2</sub> b) XRD Spectrum of N-doped-rGO/MoO<sub>2</sub>

### 3.2 Electrochemical properties of PQ<sub>23</sub>/N-doped-rGO/MoO<sub>2</sub> composite

Fig. 3 exhibits CVs of PQ<sub>23</sub>/N-doped-rGO/MoO<sub>2</sub>/GCE in phosphate buffer solution (PBS) pH=7.0. A pair of well-defined cyclic voltammetry peaks showed for PQ<sub>23</sub>/N-doped-rGO/MoO<sub>2</sub>/GCE with cathodic and anodic peak potential, E<sub>pc</sub>, E<sub>pa</sub> of 140 and 200 mV, respectively. The difference between anodic and cathodic peak potentials (ΔE<sub>p</sub>) of 60 mV is more than the 59/n mV awaited for a reversible redox reaction. As a result, the modified electrode (PQ<sub>23</sub>/N-doped-rGO/MoO<sub>2</sub>/GCE) has a quasi-reversible behavior with the modifier in an aqueous medium. Using nanocomposites, the current is increased, which indicates that the electrode reaction is faster, the electron transfer rate is increased, and the surface area is increased.

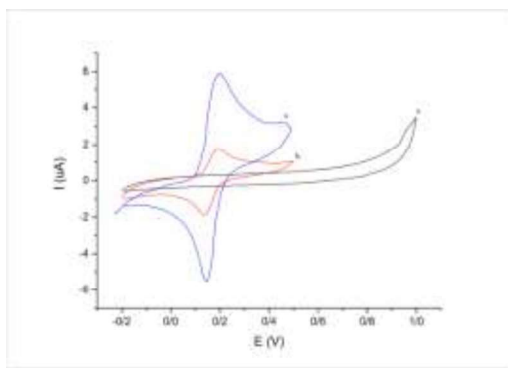


**Fig. 3.** CVs of a) bare GCE b) PQ<sub>23</sub>/GCE. c) PQ<sub>23</sub>/N-doped-rGO/MoO<sub>2</sub>/GCE. In 0.1 M PBS (pH 7.0) at v 50mV/s in -0.2 V - 0.5 V.

The effect of potential scan rate (v) on the redox system of the PQ<sub>23</sub>/N-doped-rGO/MoO<sub>2</sub>/GCE was also studied by CV (Fig. 4.). According to the results, ΔE<sub>p</sub> has increased with increasing scan rate and the anodic and cathodic currents have a linear response to the scan rate in the range of 25 to 2200 mV/s showing that the control of the redox process was diffusion independent. Surface coverage (Γ) can be calculated by Sharp method Eq. (1) [27]. Using the slope of the anodic peak current (I<sub>pa</sub>) versus of scan rate (Fig. 4a.), the surface coverage of PQ<sub>23</sub>/N-doped-rGO/MoO<sub>2</sub>/GCE was calculated as 1.22 × 10<sup>-7</sup> mol/cm<sup>2</sup> while n = 2. Also, electron-transfer rate constant (k<sub>s</sub>) can be calculated from differentiation of E<sub>pa</sub> and E<sub>pc</sub> with the log scan rate (Fig. 4b), according to laviron technique [28]. A plot of E<sub>p</sub> as a function of log v yields a straight line with a slope equal to 2.3RT/(1 - α)nF for the anodic peak (Fig. 4(d)). The values of α and k<sub>s</sub> for PQ<sub>23</sub> oxidation were determined to be 0.3 and 2.64 s<sup>-1</sup>, respectively, using such a plot and Eq. (2).

$$I_p = n^2 F A \Gamma v / 4RT \quad (1)$$

$$\log(k_s / s^{-1}) \alpha \log(1 - \alpha) \log \alpha - \log(RT / nfv) / s - \alpha(1 - \alpha) n \Delta E_p / 2.3RT \quad (2)$$

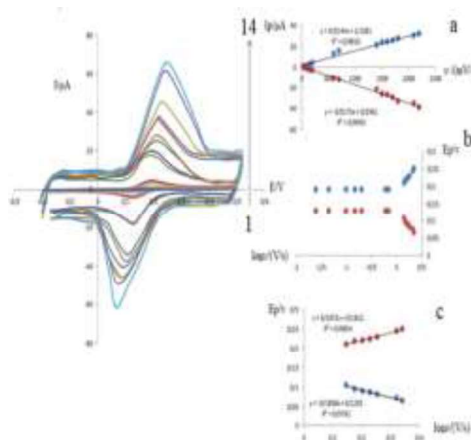


**Fig. 4.** CVs of PQ<sub>23</sub>/N-doped-rGO/MoO<sub>2</sub>/GCE in PBS (0.1 M) pH 7.0 at different v, from down to up: 25, 45, 100, 150, 200, 600, 700, 1400, 1500, 1600, 1700, 1800, 2100, 2200 mV/s. Insets: a) variation of I<sub>pa,c</sub> versus the scan rates; b) and c) E<sub>pa,c</sub> versus. log v.

The oxidation peak of the PQ<sub>23</sub>/N-doped-rGO/MoO<sub>2</sub>/GCE is pH-dependent. Therefore, the cyclic voltammetry behavior of the PQ<sub>23</sub>/N-doped-rGO/MoO<sub>2</sub>/GCE was investigated at various pHs (pHs=3.0-9.0). As the pH increased, the cathodic and anodic potentials moved toward less positive potential values. Fig. 5b shows the E<sub>p</sub>-pH plot, exhibiting the E<sub>p</sub> values as a function of pH. This plot is including of a straight line with slope = 55.6 mV/pH. The slope shows the Nernst equation for a two proton and electron transfer reaction.

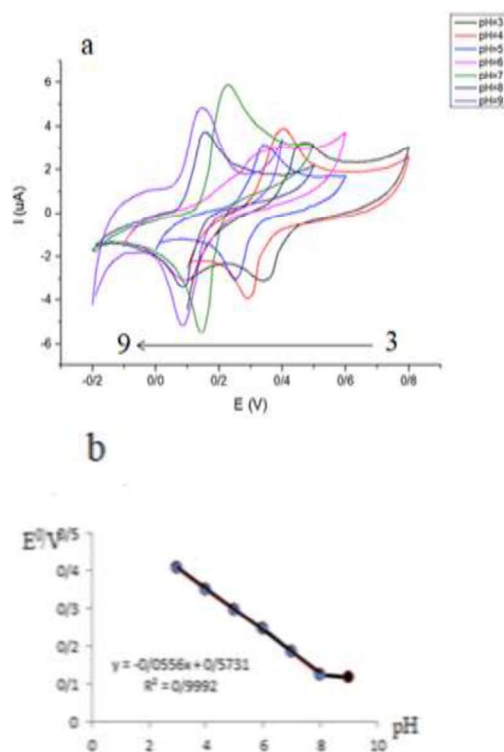


**Fig. 5.** a) CVs of PQ<sub>23</sub>/N-doped-rGO/MoO<sub>2</sub>/GCE in PBS (0.1 M), pH values from 3 to 9, scan rate 50 mV/s. b) Variation of E<sub>0</sub>V versus the pH.

EIS is a useful technique for investigating electron transfer between the electrolyte and the electrode surface. The diameter of a semicircle in a Nyquist plot is generally equal to charge transfer resistance ( $R_{ct}$ ) [29]. Fig. 6 exhibits the Nyquist diagram of the various electrodes a) bare GCE, b) modified electrode with modifier (PQ<sub>23</sub>/GCE), c) nanocomposite modified electrode (N-doped-rGO/MoO<sub>2</sub>/GCE), d) Modified electrode with modifier and nanocomposite (PQ<sub>23</sub>/N-doped-rGO/MoO<sub>2</sub>/GCE) in the Fe (CN)<sub>6</sub><sup>3-/4-</sup> (1 mM) solution containing 0.1 M KCl in Frequency range 10–10000 Hz. According to the results, the charge transfer resistance PQ<sub>23</sub>/GCE (850.5 ohm) is more than bare GCE (814.8 ohm) which can be due to weak or low modifier conductivity. In the presence of N-doped -rGO/MoO<sub>2</sub> on the surface of the bare electrode, the charge transfer resistance decreases from 814.8 ohms to 91.29 ohms and  $R_{ct}$  between the electrolyte and the electrode surface increases due to the good conductivity of the nanocomposite. In plot d, the charge transfer resistance is more than plot c due to the weak conductivity of PQ<sub>23</sub> (267.9 ohm). The results confirm the successful design of the sensor and also, show that the nanocomposite used plays an important role in the designed sensor.

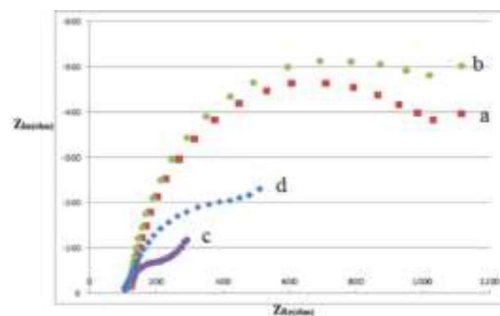
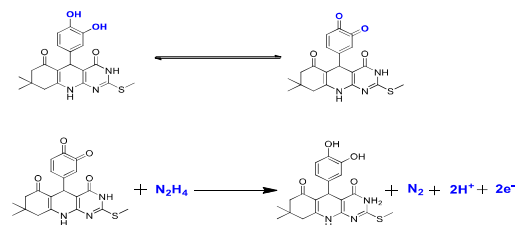


**Fig. 6.** Nyquist plots of a) bare GCE b) PQ<sub>23</sub>/GCE c) N-doped-rGo/MoO<sub>2</sub>/GCE d) PQ<sub>23</sub>/N-doped-rGO/MoO<sub>2</sub>/GCE in 1 mM [Fe(CN)<sub>6</sub>]<sup>3-/4-</sup> solution containing 0.1 M KCl. Frequency range 10 – 10000 Hz.

### 3.3 Electrochemical properties of PQ<sub>23</sub>/ N-doped-rGO/MoO<sub>2</sub> /GCE for hydrazine

To study the electrochemical behavior of hydrazine by designed sensor, bare GCE, PQ<sub>23</sub>/GCE and PQ<sub>23</sub> /N-doped-rGO/MoO<sub>2</sub>/GCE electrodes in PBS (0.1 M) pH = 8 containing a certain amount of HDZ (1 mM) with potential scan rate of 50 mV/s was investigated (Fig. 7). According to the results, the bare GCE was studied in the presence of HDZ and no oxidation peak was seen for the bare/GCE but, using the modifier (PQ<sub>23</sub>), the oxidation peak was seen in the range of 0.2 V. Therefore, the modifier (PQ<sub>23</sub>) has a good ability to improve the reaction and reduce the overvoltage of the HDZ reaction at the electrode surface. Also, in the modified electrode with N-doped-rGO/MoO<sub>2</sub> aerogel nanocomposite, the oxidation peak current is increased, which increases the response and sensitivity of the designed sensor. According to the obtained results, it was observed that the sensor oxidation current increased in the presence of hydrazine and the reduction peak was removed, the reason for this phenomenon is that with the diffusion of hydrazine from the solution to the surface of the electrode, it is converted to its reduced form by chemical reaction with hydrazine. Therefore, since all the modifiers are in reduced form, no decrease in the return is observed. These results indicate the electrocatalytic oxidation of hydrazine by the EC' mechanism (scheme 1).



**Scheme 1.** Electrocatalytic reactions mechanism for HDZ at surface of PQ<sub>23</sub>/N-doped-rGO/MoO<sub>2</sub>/GCE

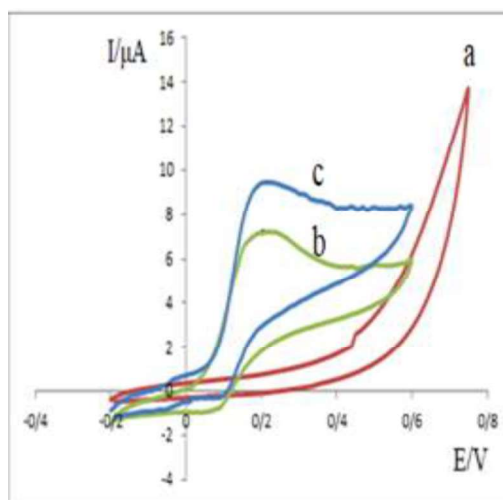


**Fig. 7.** CVs of a) bare GCE in potential range -0.2 V to 0.75 V with scan rate 50 mV/s. b) PQ<sub>23</sub>/GCE c) PQ<sub>23</sub>/N-doped-rGO/MoO<sub>2</sub>/GCE in potential range -0.2 V to 0.6 V with  $\nu$  50mV/s. in PBS (0.1 M) pH 8.0 containing 1.0 mM HDZ.

The effect of potential  $\nu$  on the electroanalytical behavior of a sensor designed for HDZ in the range of 10-50 mV/s was evaluated (Fig. 8). According to the results, it was seen that with increasing scan rate potential,  $E_{pa}$  shifts towards less negative potential values, which confirms the kinetic limitation of the electrochemical reaction. Also, the oxidation current of HDZ on the surface of the PQ<sub>23</sub>/N-doped-rGO/MoO<sub>2</sub>/GCE increases with increasing potential  $\nu$  and has a linear relationship with the square root of the potential scan rate which shows the diffusion-controlled reaction according to the Randles-Sevcik equation. The Normalized current versus the  $\nu$  (Fig. 8a) had a curve with a special shape which confirms the EC's mechanism for electrocatalytic oxidation of HDZ. In Fig. 10c, the TOEFL diagram of the TOEFL region was plotted at a  $\nu$  of 30 mV/s. Using the slope of the TOEFL diagram reported as 0.1177, the value of the transfer coefficient ( $\alpha$ ) for oxidation at the surface of the PQ<sub>23</sub>/N-doped-rGO/MoO<sub>2</sub>/GCE is about 0.5.

### 3.4 Chronoamperometric measurements

Chronoamperometric measurements for HDZ at PQ<sub>23</sub>/N-doped-rGO/MoO<sub>2</sub>/GCE were performed for the various concentration of HDZ (Fig. 9), with  $D$  (diffusion coefficient) and the Cottrell equation showing the mass transport limited current for the electrochemical reaction [30]. Fig. 9 shows, that for the various concentration of HDZ, the experimental curves of  $I$  vs.  $t^{-1/2}$  had smooth lines, according to the Cottrell equation and slope ( $I$  vs.  $t^{-1/2}$ ) the average value of the  $D$  was estimated to be  $5.89 \times 10^{-6} \text{ cm}^2 \text{ s}^{-1}$ .

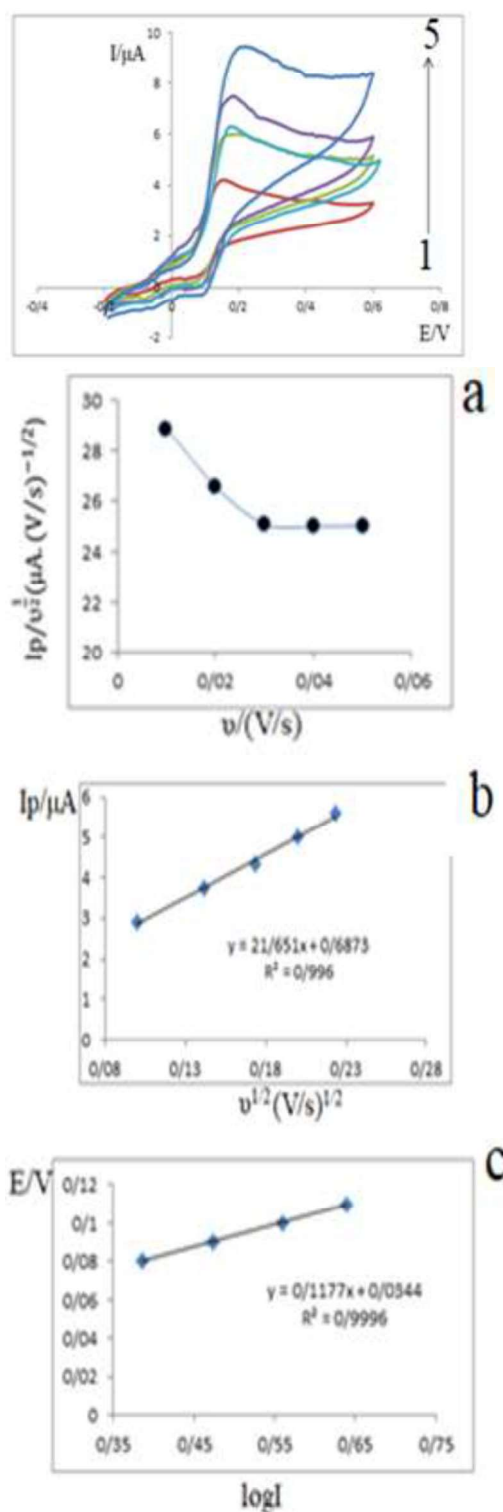


**Fig. 8.** CVs of PQ<sub>23</sub>/N-doped-rGO/MoO<sub>2</sub>/GCE in PBS (0.1 M) pH 8.0 containing 1.0 mM HDZ at scan rates from down to up: 10, 20, 30, 40, 50 mV/s. a) Variation of normalized current versus the scan rates. b) Anodic peak current versus  $\nu^{1/2}$ . c) Tafel plot from the tafel area of voltammogram recorded at scan rate of 30 mV/s.

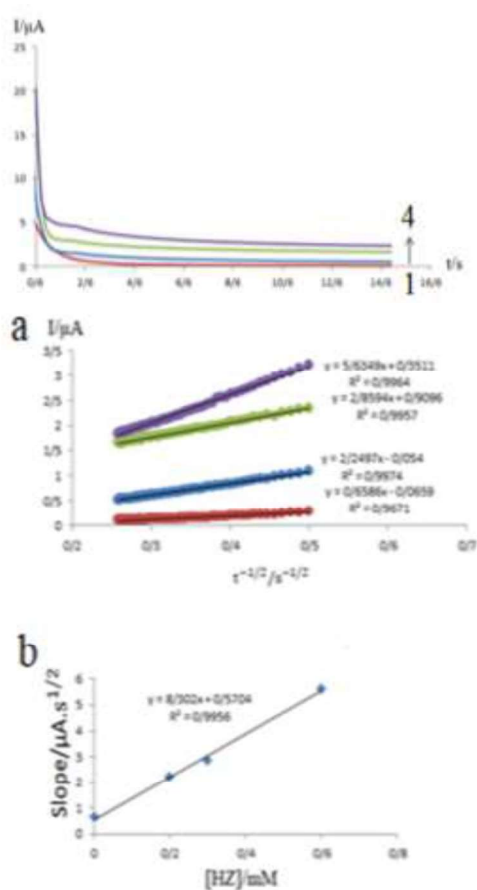


**Fig. 9.** Chronoamperograms obtained at PQ<sub>23</sub>/N-doped-rGO/MoO<sub>2</sub>/GCE in PBS (0.1 M) pH 8.0 for different concentration of HDZ at a potential step of 0.23 V. The numbers 1-4 correspond to 0, 0.2, 0.3, 0.6 mM of HDZ. Insets: a) plots of I VS.  $t^{-1/2}$ . b) plot of the slope of the straight lines versus the HDZ concentration.

### 3.5 Plotting the calibration curve and calculating the detection limit

Fig. 10 shows DPV curves for various concentrations of HDZ at PQ<sub>23</sub>/N-doped-rGO/MoO<sub>2</sub>/GCE in PBS (pH 8.0), with increasing concentration of hydrazine, the oxidative current has increased. According to the results, the calibration plot has two linear regions with different slopes and concentrations of 25-200  $\mu$ M and 200-1000  $\mu$ M. At concentrations above 200  $\mu$ M, the slope of the line is less than the first region and the sensitivity is lower, because the presence of nitrogen gas in high concentrations affects the diffusion of HDZ to the electrode surface. As a result, the slope of the curve decreases, but this phenomenon has no significant effect at low concentrations. Therefore, the first region was applied to determine the detection limit and the detection limit was 4.2  $\mu$ M.

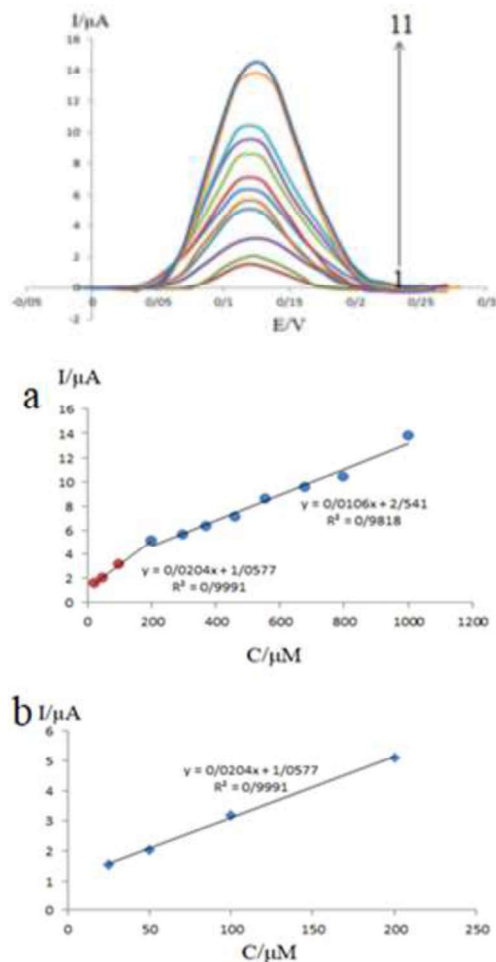


**Fig. 10.** DPVs of PQ<sub>23</sub>/N-doped-rGO/MoO<sub>2</sub>/GCE in PBS (0.1 M) pH 8.0 containing various concentrations of HDZ (1 to 11 corresponds to 25, 50, 100, 200, 300, 371, 461, 557, 678, 800, 1000  $\mu$ M.) Insets: a) Calibration plot of HDZ b) plot of 25-200  $\mu$ M from a.

### 3.6 Interference study

The selective response is an essential characteristic for sensors that probe the sensor-selective response to an analyte in the presence of other species. The influence of different foreign species on the determination of 0.1 M hydrazine. The tolerance limit was taken as the maximum concentration of the foreign species, which caused an approximately  $\pm 5\%$  relative error in the determination. The oxidation current in the absence of interference species and in the presence of interference species, different concentrations of potassium chloride, sodium bicarbonate, Copper (II) nitrate, sodium carbonate and sodium nitrate was investigated. These results revealed a good selectivity of the PQ<sub>23</sub>/N-doped-rGO/MoO<sub>2</sub>/GCE nanocomposite to detect HDZ in complicated media.

### 3.7 Real samples measurement

To investigate the performance of the designed sensor (PQ<sub>23</sub>/N-doped-rGO/MoO<sub>2</sub>/GCE), a drinking water sample was prepared and mixed with PBS (pH = 8) in a ratio of 1:1. Then, different concentrations of HDZ were prepared from this solution and examined by DPV (Each concentration was repeated three times). Finally, the average current in each concentration was placed in the line equation of the relevant area and the desired concentration was calculated. The results were reported in Table (1).

**Table 1.** The application of PQ<sub>23</sub>/N-doped-rGO/MoO<sub>2</sub>/GCE for determination of HDZ in water samples.

Hydrazin Added (μM)	Found (μM)	Recovery (%)	RSD (%)
0	-	-	-
110	106.5	96.8	1.0
146	141.3	96.8	2.8
240	245.4	102.2	0.9
360	381.9	106.1	4.1
480	486.6	101.4	2.1

### 3.8 The reproducibility and repeatability of PQ<sub>23</sub>/N-doped-rGO/MoO<sub>2</sub>/GCE

To study the reproducibility of the sensor designed by DPV in a solution containing HDZ on different days and RSD = 5.8% was reported for this sensor. To investigate the repeatability of the sensor designed with DPV in three solutions containing HDZ with the same concentration was examined by one electrode and RSD = 5.3% was obtained.

## 4. CONCLUSION

In summary, to measure HDZ, an electrochemical sensor was prepared using a glass-modified carbon electrode with a PQ<sub>23</sub> modifier and N-doped reduced graphene aerogel/ molybdenum oxide nanorods. The aerogel used increases the conductivity and fast electron transfer and plays an important role in the designed electrochemical sensor. For the designed sensor, the effect of pH, kinetic and thermodynamic parameters, the effect of the intrusive species for the measurement of HDZ, and the reproducibility and repeatability were investigated. A detection limit of 4.2 μM and a linear range of 25.0-1000.0 μM were reported to measure HDZ with designed sensor.

### Acknowledgements

The financial support of this research by Yazd University Research Council is gratefully Acknowledged.

## REFERENCES

- [1] J. Kavitha, M. Devendiran, K.K. Kumar, S.S. Narayanan, Electrochemical Sensor for the Determination of Hydrazine Using Mwcnt/Dopamine Dithiocarbamate Modified Electrode, *Int. J. Sci. Res. Sci. Technol.* 6 (2017) 227–232.
- [2] M. Mazloum-ardakani, Z. Alizadeh, L. Hosseinzadeh, An Electrochemical Sensor Based on Functionalized Carbon Nanotube with Pyrazole Derivative for Determination of Hydrazine, *IJAC*, 6 (2019) 49-56
- [3] D. Afzali, H. Karimi-Maleh, M.A. Khalilzadeh, Sensitive and selective determination of phenylhydrazine in the presence of hydrazine at a ferrocene-modified carbon nanotube paste electrode, *Environ. Chem. Lett.* 9 (2011) 375–381.
- [4] S. Kurbanoglu, M.A. Unal, S.A. Ozkan, Recent developments on electrochemical flow injection in pharmaceuticals and biologically important compounds, *Electrochim. Acta.* 287 (2018) 135–148.
- [5] K. Tašev, I. Karadjova, T. Stafilov, Determination of inorganic and total arsenic in wines by hydride generation atomic absorption spectrometry, *Microchim. Acta.* 149 (2005) 55–60.
- [6] R. Gilbert, R. Rioux, Ion Chromatographic Determination, (1984) 106–109.
- [7] D.S. Kosyakov, A.S. Amosov, N. V. Ul'yanovskii, A. V. Ladesov, Y.G. Khabarov, O.A. Shpigun, Spectrophotometric determination of hydrazine, methylhydrazine, and 1,1-dimethylhydrazine with preliminary derivatization by 5-nitro-2-furaldehyde, *J. Anal. Chem.* 72 (2017) 171–177.
- [8] M.H. Nagaoka, H. Nagaoka, K. Kondo, H. Akiyama, T. Maitani, Measurement of a genotoxic hydrazine, agaritine, and its derivatives by HPLC with fluorescence derivatization in the agaricus mushroom and its products, *Chem. Pharm. Bull.* 54 (2006) 922–924.
- [9] B. Fang, C. Zhang, W. Zhang, G. Wang, A novel hydrazine electrochemical sensor based on a carbon nanotube-wired ZnO nanoflower-modified electrode, *Electrochim. Acta.* 55 (2009) 178–182.
- [10] Y. Zhu, P. Chandra, Y.B. Shim, Ultrasensitive and selective electrochemical diagnosis of breast cancer based on a hydrazine-Au nanoparticle-aptamer bioconjugate, *Anal. Chem.* 85 (2013) 1058–1064.
- [11] W. Zhao, X.Q. Wu, Z.Q. Lu, W.J. Hou, H.X. Li, Electrochemical studies of chloroperoxidase on poly-l-lysine film modified GC electrode, *Chinese Chem. Lett.* 21 (2010) 93–96.

- [12] J.A. Oh, H.S. Shin, Simple determination of hydrazine in waste water by headspace solid-phase micro extraction and gas chromatography-tandem mass spectrometry after derivatization with trifluoro pentanedione, *Anal. Chim. Acta.* 950 (2017) 57–63.
- [13] M. Mazloum-Ardakani, Z. Alizadeh, F. Sabaghian, B.B.F. Mirjalili, N. Salehi, Novel Fe<sub>2</sub>O<sub>3</sub>@CeO<sub>2</sub> Core-shell-based Electrochemical Nanosensor for the Voltammetric Determination of Norepinephrine, *Electroanalysis.* 32 (2020) 455–461.
- [14] J.J. Hernández Rosas, R.E. Ramírez Gutiérrez, A. Escobedo-Morales, E. Chigo Anota, First principles calculations of the electronic and chemical properties of graphene, graphane, and graphene oxide, *J. Mol. Model.* 17 (2011) 1133–1139.
- [15] D.A.C. Brownson, G.C. Smith, C.E. Banks, Graphene oxide electrochemistry: The electrochemistry of graphene oxide modified electrodes reveals coverage dependent beneficial electrocatalysis, *R. Soc. Open Sci.* 4 (2017).
- [16] R. Kumar, S. Sahoo, E. Joanni, R.K. Singh, K. Maegawa, W.K. Tan, G. Kawamura, K.K. Kar, A. Matsuda, Heteroatom doped graphene engineering for energy storage and conversion, *Mater. Today.* 39 (2020) 47–65.
- [17] J. Liu, Q. Ma, Z. Huang, G. Liu, H. Zhang, Recent Progress in Graphene-Based Noble-Metal Nanocomposites for Electrocatalytic Applications, *Adv. Mater.* 31 (2019) 1–20.
- [18] W. Hua, H.H. Sun, F. Xu, J.G. Wang, A review and perspective on molybdenum-based electrocatalysts for hydrogen evolution reaction, *Rare Met.* 39 (2020) 335–351.
- [19] H. Ren, S. Sun, J. Cui, X. Li, Synthesis, functional modifications, and diversified applications of molybdenum oxides micro-/nanocrystals: A review, *Cryst. Growth Des.* 18 (2018) 6326–6369.
- [20] J. Xu, K. Xu, Y. Han, D. Wang, X. Li, T. Hu, H. Yi, Z. Ni, A 3D porous graphene aerogel@GOx based microfluidic biosensor for electrochemical glucose detection, *Analyst.* 145 (2020) 5141–5147.
- [21] R. Li, T. Yang, Z. Li, Z. Gu, G. Wang, J. Liu, Synthesis of palladium@gold nanoalloys/nitrogen and sulphur-functionalized multiple graphene aerogel for electrochemical detection of dopamine, *Anal. Chim. Acta.* 954 (2017) 43–51.
- [22] L. Ruiyi, L. Ling, B. Hongxia, L. Zaijun, Nitrogen-doped multiple graphene aerogel/gold nanostar as the electrochemical sensing platform for ultrasensitive detection of circulating free DNA in human serum, *Biosens. Bioelectron.* 79 (2016) 457–466.
- [23] X. Niu, W. Zhang, Y. Huang, L. Wang, Z. Li, W. Sun, An electrochemical sensing platform amplified with a Au@Ag nanoparticle-decorated three-dimensional N-doped graphene aerogel for ultrasensitive determination of baicalein, *New J. Chem.* 44 (2020) 15975–15982.
- [24] Y. Xie, X. Tu, X. Ma, M. Xiao, G. Liu, F. Qu, R. Dai, L. Lu, W. Wang, In-situ synthesis of hierarchically porous polypyrrole@ZIF-8/graphene aerogels for enhanced electrochemical sensing of 2, 2-methylenebis (4-chlorophenol), *Electrochim. Acta.* 311 (2019) 114–122.
- [25] S. Saadat, B. Bi, F. Mirjalili, N. Salehi, efficient synthesis of and indenopyrido [ 2 , 3 - d ] pyrimidine derivatives in the presence of Fe<sub>3</sub>O<sub>4</sub> @ nano-cellulose / Sb ( V ) as bio-based magnetic nano-catalyst, 4 (n.d.) 1–16.
- [26] A. Bhaskar, M. Deepa, T.N. Rao, U. V. Varadaraju, Enhanced nanoscale conduction capability of a MoO<sub>2</sub>/Graphene composite for high performance anodes in lithium ion batteries, *J. Power Sources.* 216 (2012) 169–178. doi:10.1016/j.jpowsour.2012.05.050.
- [27] M. Sharp, M. Petersson, Preliminary note P R E L I M I N A R Y D E T E R M I N A T I O N S O F E L E C T R O N T R A N S F E R K I N E T I C S I N V O L V I N G F E R R O C E N E C O V A L E N T L Y A T T A C H E D T O A P L A T I N U M S U R F A C E, 95 (1979) 123–130.
- [28] E. Laviron, Surface linear potential sweep voltammetry. Equation of the peaks for a reversible reaction when interactions between the adsorbed molecules are taken into account, *J. Electroanal. Chem.* 52 (1974) 395–402.
- [29] D. Rao, Q. Sheng, J. Zheng, Preparation of flower-like Pt nanoparticles decorated chitosan-grafted graphene oxide and its electrocatalysis of hydrazine, *Sensors Actuators, B Chem.* 236 (2016) 192–200.
- [30] M. Mazloum-Ardakani, H. Beitollahi, M.K. Amini, F. Mirkhalaf, B.F. Mirjalili, A highly sensitive nanostructure-based electrochemical sensor for electrocatalytic determination of norepinephrine in the presence of acetaminophen and tryptophan, *Biosens. Bioelectron.* 26 (2011) 2102–2106.

## COPYRIGHTS



© 2022 by the authors. Licensee PNU, Tehran, Iran. This article is an open access article distributed under the terms and conditions of the Creative Commons Attribution 4.0 International (CC BY4.0) (<http://creativecommons.org/licenses/by/4.0>)

## بررسی الکتروشیمیایی و اندازه‌گیری ولتامتری هیدرازین با استفاده از الکتروود کربن شیشه‌ای اصلاح شده

محمد مظلوم اردکانی\*، حامد اعرابی اردکانی، زهرا علیزاده، مهنوش حق شناس، فاطمه فرید،

فاطمه سادات حسینی خواه، بی بی فاطمه میر جلیلی

بخش شیمی، دانشکده علوم، دانشگاه یزد، یزد، ایران

تاریخ دریافت: ۲۶ دی ۱۴۰۰ تاریخ پذیرش: ۲۴ بهمن ۱۴۰۰

### چکیده

در این مطالعه، برای سنجش هیدرازین یک حسگر الکتروشیمیایی با استفاده از الکتروود کربن شیشه‌ای اصلاح شده برپایه اصلاحگر آلی ۵-(۳-۴-دی‌هیدروکسی‌فنیل)-۸-۸-دی‌متیل-۲-(متیل‌تیو)-۷-و ۹-۱۰-تترا‌هیدروپیریمیدو[۵,۴b-کینولون-۴ و ۳-(H,5SH)-دیون (PQ23) و نانوکامپوزیت آیروزل گرافن اکسید کاهش یافته آلیبده شده با نیتروژن/نانو میله‌های مولیبدن اکسید طراحی شد. برای بررسی ساختار و ترکیب نانوذرات سنتزی از SEM، XRD، EDS و MAP استفاده شد. الکتروود اصلاح شده با طیف‌بینی امپدانس الکتروشیمیایی (EIS) مورد بررسی قرار گرفت و بهبود انتقال الکترون به دلیل رسانایی خوب نانوکامپوزیت تایید شد. با استفاده از ولتامتری چرخه‌ای اکسایش هیدرازین مورد بررسی قرار گرفت و کاهش اضافه پتانسیل و افزایش جریان در سطح الکتروود اصلاح شده مشاهده و همچنین ضریب انتقال اصلاحگر برای اکسایش هیدرازین ۰/۵ محاسبه شد. با استفاده از ولتامتری تپی تفاضلی غلظت‌های مختلف از هیدرازین در سطح الکتروود اصلاح شده بررسی و حد تشخیص ۴,۲ میکرومولار و گستره خطی ۱۰۰۰-۲۵,۰ میکرومولار برای روش پیشنهادی گزارش شد.

### واژه‌های کلیدی

حسگر الکتروشیمیایی؛ الکتروود کربن شیشه‌ای؛ هیدرازین. نانوکامپوزیت.